SANITAS: JURNAL TEKNOLOGI DAN SENI KESEHATAN
ISSN : 1978-8843 (*PRINT*) / 2615-8647 (*ONLINE*) **Vol. 16 No. 2: 98 - 108**

SIMULATION OF AN ADAPTIVE X-RAY CONTROL INTERFACE USING AUTOMATED ANTHROPOMETRY AND THERMAL MOTION DETECTION

Fatahah Dwi Ridhani[1*], Winda Wirasa[1], Wike Kristianti[1]

[1] Poltekkes Kemenkes Jakarta II, Jakarta, Indonesia

*Corresponding E-mail: ridhani@poltekkesjkt2.ac.id

Submitted: 21st December 2025; Accepted: 31 December 2025

http://doi.org/10.36525/sanitas.2025.553

ABSTRACT

Manual determination of radiographic exposure parameters often results in inconsistent radiation dosing due to subjective assessment of patient body habitus. This study presents the design and component-level simulation of an automated control interface that regulates tube voltage (kV) and current-time (mAs) based on patient Body Mass Index (BMI). The system architecture integrates a sensor fusion array comprising a VL53L0X Time-of-Flight sensor for non-contact vertical ranging, a strain gauge load cell for gravimetric acquisition, and an AMG8833 thermal grid to enforce a stillness protocol before measurement. A central microcontroller processes these inputs using a combined linear and quadratic algorithm to derive optimal exposure settings, incorporating a variable correction factor for machine-specific characteristics. The control logic was validated through an electronic simulation of a capacitor discharge X-ray generator. Results demonstrate robust performance, with biometric acquisition achieving gravimetric accuracy exceeding 97% and absolute vertical precision. Furthermore, the simulated high-voltage control loop successfully mapped five distinct BMI categories to their corresponding target voltages (57kV–69kV) with a deviation of less than 2%. This research confirms the analytical feasibility of utilizing automated anthropometry to drive high-voltage circuitry, offering a technological pathway to reduce operator error and standardize radiation protection in diagnostic imaging.

Keywords: *Radiographic Simulation, Biometric Automation, Adaptive Control*

INTRODUCTION

Body Mass Index (BMI) serves as a primary metric for estimating adiposity by analyzing the ratio of height to weight(1,2). In clinical settings, medical practitioners utilize this calculation to classify patients into distinct categories, ranging from underweight to obese status(3). While common in general health assessments, this metric holds specific relevance in the field of diagnostic radiography.

The physical dimensions of a patient are a critical determinant in X-ray imaging physics. As body thickness increases, tissue attenuation rises, necessitating a proportional increase in photon energy(4). Empirical evidence demonstrates a direct correlation between a patient's BMI and the kilovoltage required for optimal penetration(5). Consequently, inaccurate parameter selection can compromise diagnostic image quality and inadvertently subject individuals to excessive radiation exposure(6). Therefore, integrating BMI into dose determination protocols is vital for patient safety and is foundational for calculating Size-Specific Dose Estimates (SSDE) in complex modalities(7,8). Despite this, conventional workflows often rely on manual, subjective parameter adjustments by operators, increasing the margin for error.

In recent years, the integration of wireless technology has modernized radiographic control systems. Research by Wijaya and Sukwono introduced wireless mechanisms for adjusting Kilovolt (kV) settings remotely(9), a concept they later expanded to include Milliampere (mA) regulation(10). These innovations streamline clinical operations. Parallel efforts have prioritized safety; for instance, Sulistiyadi et al. engineered a Bluetooth-based exposure switch to distance operators from the radiation source(11). Similarly, Loniza et al. constructed prototypes specifically for wireless kV modulation(12). These engineering solutions collectively reduce the physical workload on radiographers while reinforcing radiation protection protocols.

Concurrently, the automation of anthropometric measurements has evolved significantly. Early automated BMI calculators(13) have been refined by researchers like Owolabi et al., who emphasized cost-effective architectural designs(14). Contemporary iterations have adopted mobile integration, with Android-based systems becoming prevalent(15). Furthermore, computational logic has improved, with some devices employing fuzzy logic algorithms for body composition analysis(16) or leveraging the Internet of Things (IoT) for decentralized data processing(17). To address hygiene concerns and measurement precision, recent studies have also successfully implemented non-contact ultrasonic sensors(18,19).

However, a technological disconnect remains. Although automated BMI tools and wireless X-ray controllers exist, they typically operate as isolated systems. The data transfer between patient measurement and machine setting remains largely manual. To bridge this gap, this study proposes a simulated interface for automatic kV control, as an add-on to the current electromedical devices setup(20). By directly utilizing BMI data as a control input, the system aims to automate the modulation of X-ray parameters. This design seeks to ensure that radiation dosage is both precise and strictly proportional to individual patient morphology.

The reduction of motion artifacts represents a critical urgency in modern radiography. Slight patient movements during biometric measurement can lead to calculation errors, resulting in suboptimal exposure settings. Worse, unnoticed motion during the pre-exposure phase necessitates image retakes, significantly escalating the cumulative radiation dose. To mitigate this risk, this study engineered a specialized anthropometric module. The system utilizes the VL53L0X Time-of-Flight sensor to achieve sub-millimeter precision in height acquisition. Crucially, this sensor is paired with an AMG8833 Grid-EYE infrared array. This thermal integration serves a vital safety protocol. It detects the specific thermal signature of a living subject, distinguishing a patient from inanimate objects(21). Furthermore, the thermal array continuously monitors the subject's heat map to verify physical stillness, effectively locking the system until the patient is stationary.

Data from this bi-modal sensor array feeds directly into the central processing unit. Here, the raw anthropometric inputs are synthesized to derive the precise Kilovolt (kV) and Milliampere-seconds (mAs) targets. A distinct feature of this architecture is the inclusion of a variable correction factor. This algorithm adjusts the output to account for the unique degradation characteristics and efficiency profiles of specific X-ray machine brands. To validate the safety and reliability of this control logic, the entire workflow was not merely calculated but rigorously tested against a high-fidelity electronic simulation. This simulation modeled a high-voltage capacitor discharge circuit, proving the system's capacity to drive the heavy electrical loads required for actual X-ray generation.

RESEARCH METHOD

A. Experimental Setup and Sensor Fusion

The data acquisition front-end is designed for non-contact precision with web-based display and user interfaces. The user should select one of the preload x-ray machines listed, that had been calibrated in their stations. Types of photos can also be selected, like thorax PA/AP, thorax lateral, abdomen AP (BNO/KUB) or Lumbosacral. This simulation utilizes the Thorax PA projection protocol as the baseline reference, as it represents the most prevalent radiographic examination in routine clinical practice.

A VL53L0X Time-of-Flight (ToF) sensor handles vertical ranging to determine patient height. Simultaneously, an AMG8833 thermal grid serves a dual purpose. It confirms subject presence through thermal signature verification and monitors temporal stability to ensure patient stillness. This sensor fusion strategy minimizes motion artifacts before the calculation phase begins. The core logic is processed by an ESP32 microcontroller, chosen for its dual-core capability to handle sensor telemetry and logic processing in parallel. It also served as a web server on which the user inputs settings. Simultaneously, gravimetric data acquisition is handled by a full-bridge single cantilever 200 kg maximum rated strain gauge load cell integrated into the patient platform. As the raw differential signal from the load cell is microscopic, an HX711 interface module is interposed. This 24-bit analog-to-digital converter performs critical signal amplification, delivering high-resolution mass data to the processor.

To minimize background noise and ensure precise vertex targeting, the VL53L0X sensor was configured with a narrowed Region of Interest (ROI). By limiting the active SPAD array to the central optical axis, the effective Field of View (FoV) was reduced from the standard 25 degrees to approximately 15 degrees. This optical constriction prevents false readings from peripheral objects, ensuring the distance measurement corresponds strictly to the patient's cranial apex. The AMG8833 was read at its maximum throughput at 10 measurements per second, with simple averaging of its measurements to imply stillness of object, and neglecting the usually normal human body temperature as tested. In the future, it would be possible to use machine learning to determine the correct object by using the AMG8833 array outputs(22).

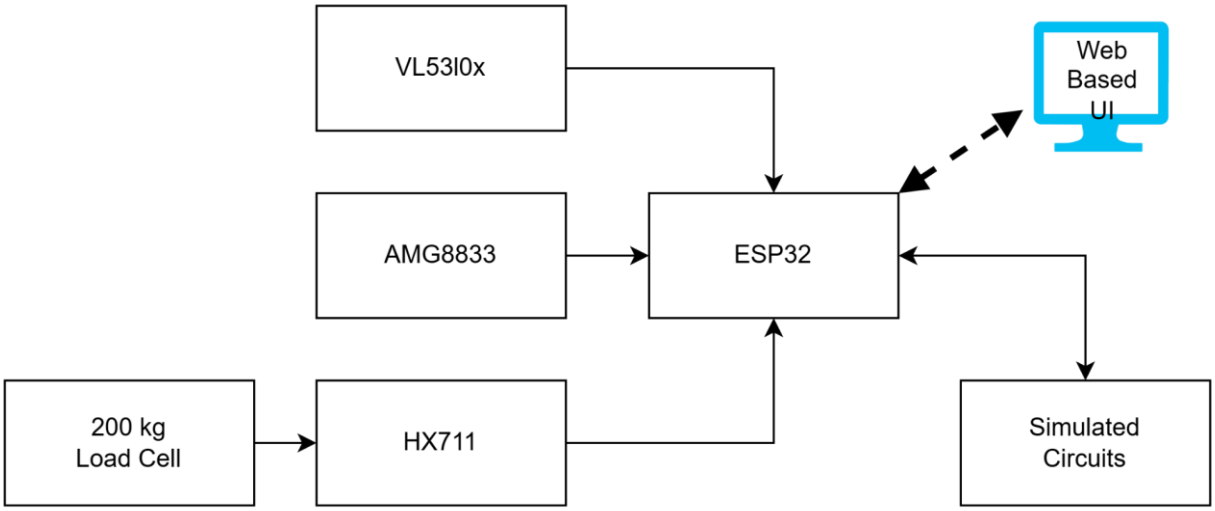

Figure 1. Operational flow from sensor acquisition to actuator control.

B. Algorithm Principle: BMI to Exposure Parameters

The central processing unit executes a multi-stage algorithm shown in figure 2. First, the users select a particular x-ray machine that has been calibrated and the data known and its type of photos to be taken. Anthropometric inputs are synthesized into a precise Body Mass Index (BMI) value. This value drives two distinct mathematical models to determine the exposure parameters. Tube voltage (kV) follows a linear trajectory, increasing proportionally to match average tissue density. In contrast, the current-time product (mAs) adheres to a quadratic function. This accounts for the non-linear attenuation of photons as body mass increases. Crucially, the algorithm applies a distinct "efficiency coefficient" at this stage. This variable adjusts the final output to compensate for the specific aging characteristics and output efficiency of the target X-ray machine that was calibrated and correction data currently available. Currently, the mapping function was a dummy one, using common values used in the past experiments, but it could be corrected after each x-ray machine listed had been calibrated. The output value could be simulated on the circuit. This circuit was also closed loop controlled for performance measurements.

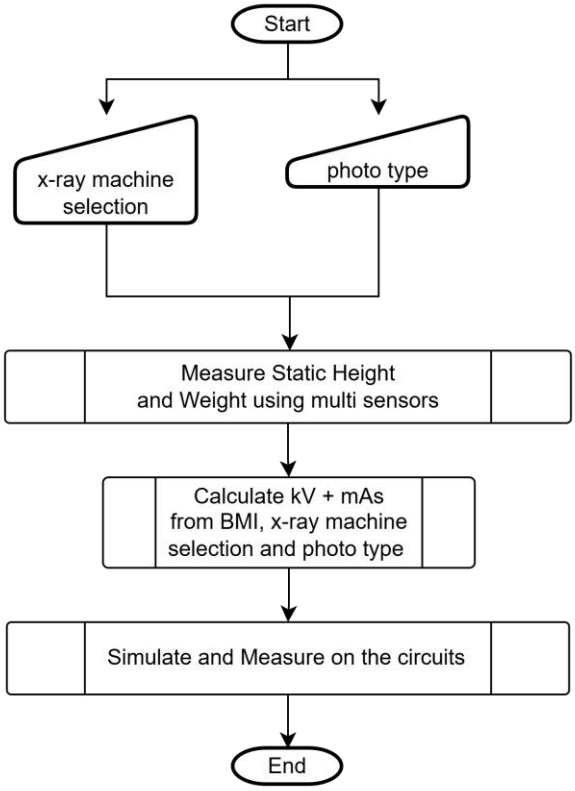

Figure 2. Determination of kV and mAs values with integrated correction factors.

C. Circuit Control and Simulation

The electrical simulation models a Capacitor-Discharge (CD) generator architecture. The high-voltage interface relies on a closed-loop feedback mechanism. A simulated solid-state relay manages the charging cycle of the main capacitor bank. To ensure safety, a voltage divider network provides real-time telemetry to the controller. This feedback loop ensures the charging process terminates precisely when the calculated target potential is reached. For the exposure phase, the system simulates the rapid discharge of energy into the X-ray tube load. This simulation validates the system's ability to maintain voltage stability even under heavy current demands. This circuit, as shown in figure 3, consists of high voltage DC source, magnetic contactor or relay, NPN transistors of D400, capacitors of 680µF/250V, resistors of 10kΩ, dummy load and optoisolator PC817 that connects to the microcontroller outputs. The microcontroller controls charge and discharge, labeled FillCap and DrainCap. The DC source used was $150V_{DC}$. The Expose was to control simulating x-ray exposure, using a dummy load that consisted of 10kΩ resistor and LED. The lower circuit was going to microcontroller ADC input, with V_{CAP} was 1:25 of V_{C2+C3}.

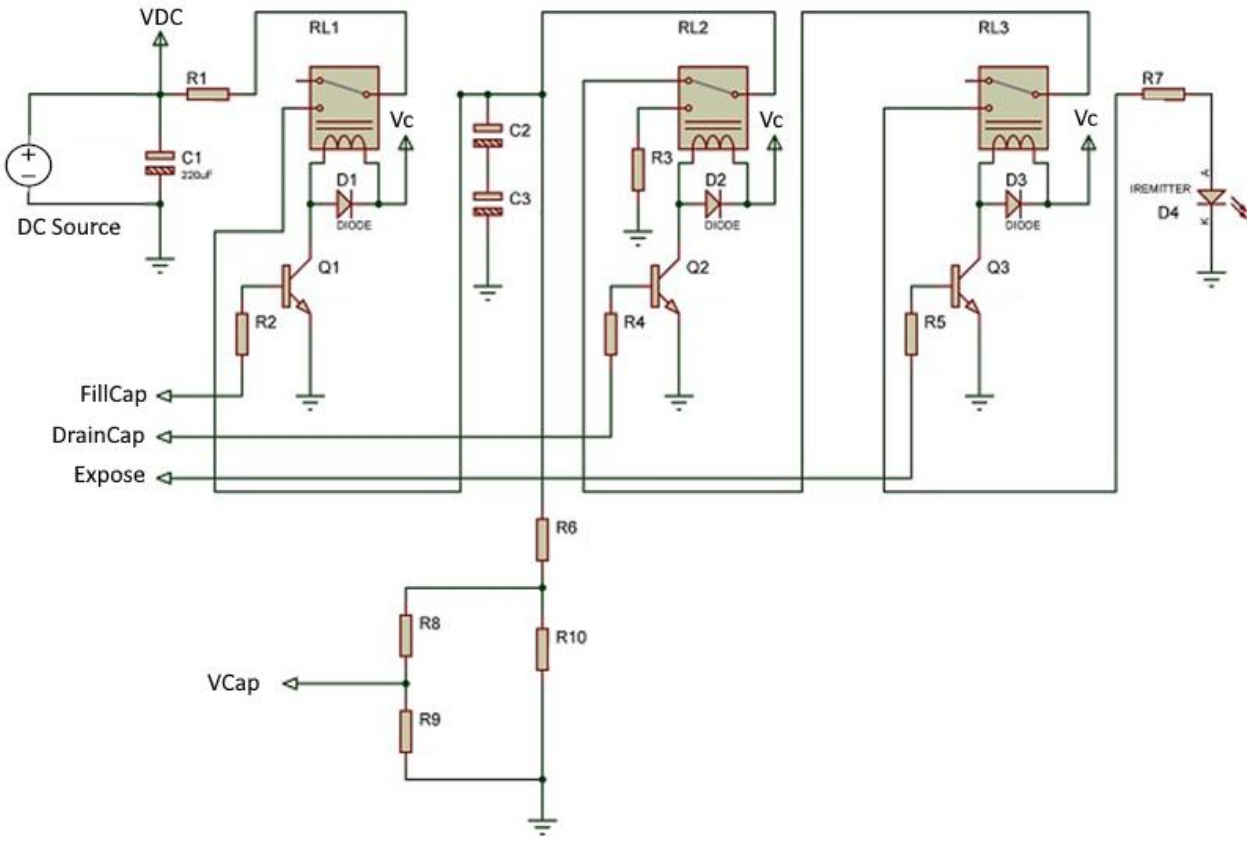

Figure 3. Detailed schematic of the charging control and discharge simulation circuit.

D. Physical Design Architecture

The sensor array is housed in an upright platform, with the VL53L0X and AMG8833 at the top platform with the height 200 cm from top of the lower platform and shown at figure 4. Those sensors were placed as close as possible and the load cell at the lower platform was designed to be single hinged to reduce flexure effect. The current range of height measurement was set to simulate average adults between 150 to 190 cm. This means VL53L0X was going to measure between 10-40 cm of range. The target was a static dummy type, with an area of obstructions wide enough to contain all of the laser cone field of views typical of a ranged measurement sensor(23).

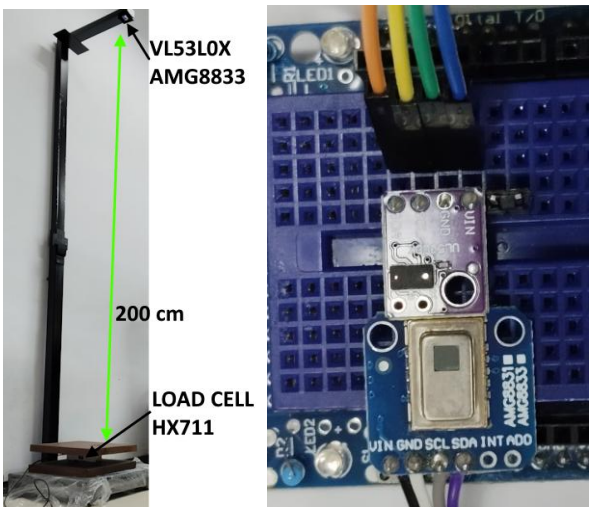

Figure 4. Proposed physical enclosure and sensor placement.

RESULTS AND DISCUSSION

The experimental protocol commenced with the selection of the "Thorax AP" projection mode. The system calibration profile was set to "Dummy 1" to simulate a standard generic X-ray generator. A critical initial phase involved the validation of subject stillness. The AMG8833 thermal grid sensor was utilized for this purpose. The algorithm required the subject's thermal heat map to remain static for a minimum threshold of 0.5 seconds. This "thermal lock" prevented premature measurement. Once stability was confirmed, the VL53L0X optical sensor activated. It aggregated distance data for a window of up to 5 seconds. This temporal averaging filtered out transient noise.

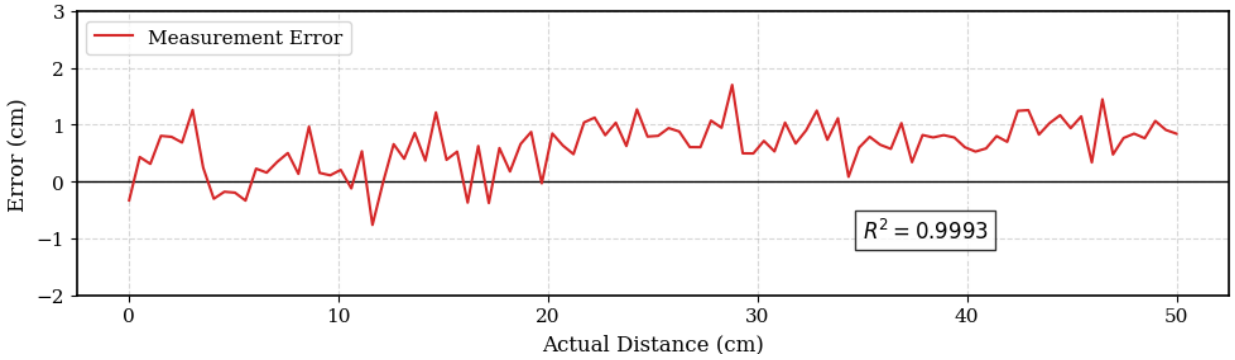

Figure 5. Linearity and Error Analysis of the Optical Ranging Module

Figure 5 presents the performance characteristics of the VL53L0X sensor within the critical 0-50 cm operational range. It details the residual error. The data points closely adhere to the ideal yielding a determination coefficient (R^2) of >0.99. This confirms a high degree of linearity. The measurements exhibit a slight positive bias averaging approximately +0.5 cm as the distance increases. The overall error magnitude remains consistently below ±1.5 cm. This precision is sufficient for the application's

requirement of distinguishing patient height for BMI categorization, where a standard error tolerance of ±1 cm is clinically acceptable.

Simultaneously, the system evaluated the patient's mass using the integrated load cell. The raw data from the HX711 interface was converted into kilogram units. Five distinct test subjects were measured to cover a broad range of body types. The recorded data compared the system's reading against a calibrated medical scale.

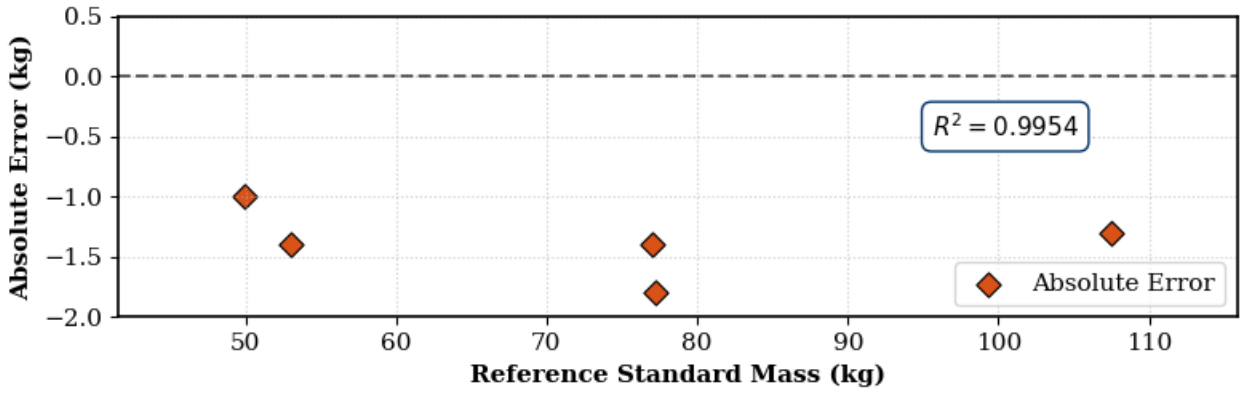

Figure 6. Correlation analysis between the prototype mass sensor readings and the calibrated standard.

Figure 6 visualizes the performance of the mass acquisition system. The experiments used 5 samples, that was 49.9, 53.0, 77.0, 77.2, and 107.5kg. The data points have a linear progression ($R^2 \approx 0.99$). This indicates that the strain gauge responds proportionally across different loads. However, a slight offset is visible in the lower mass ranges. The largest deviation, with an accuracy of 97.4%, and at heavier loads reaching 98.8%. This suggests the sensor is slightly more efficient at higher compression levels. Despite these minor variances, the average accuracy remains high.

The final stage of the experiment validated the core control loop. The microcontroller synthesized the height and weight data into a BMI value. Based on this value, the algorithm assigned a target Kilovolt (kV) setting. This digital target was converted into an analog signal to drive the simulation circuit. A voltage divider then fed the signal back to the ADC for verification.

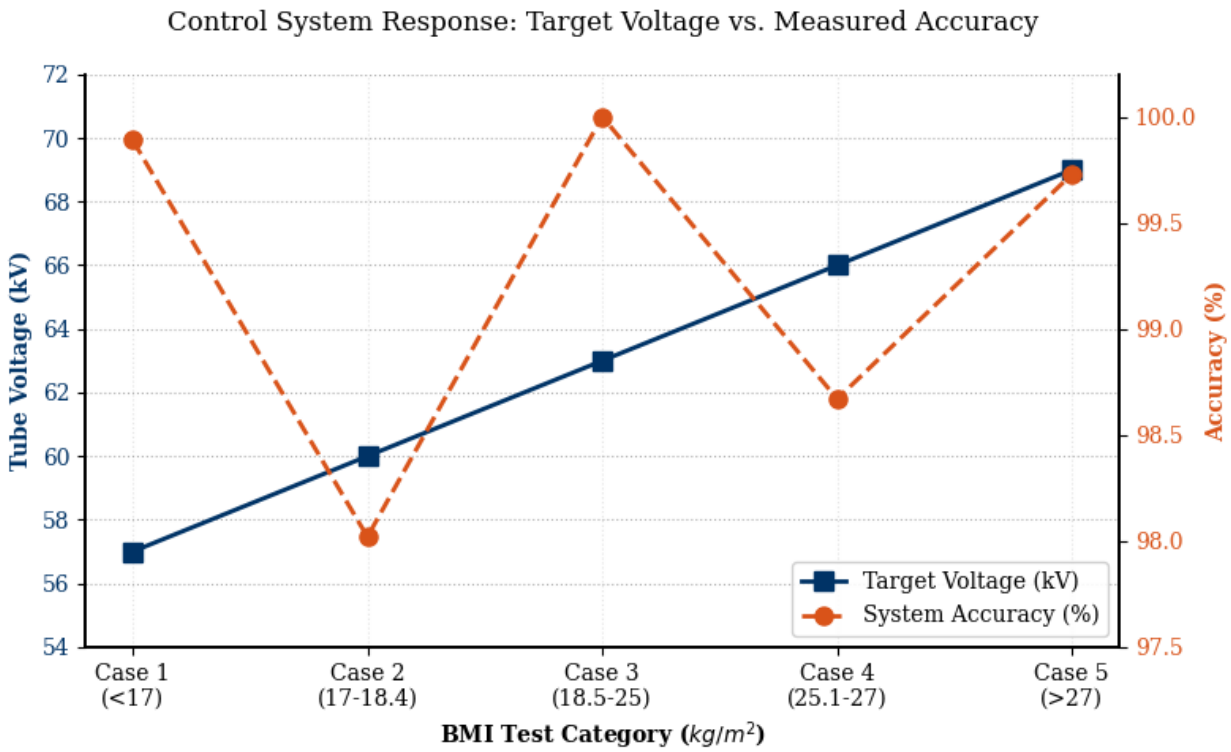

Figure 7. Discrete voltage response across the five programmed BMI categories.

Figure 7 illustrates the dual performance metrics of the electronic control logic across the five tested BMI categories. The left vertical axis (solid blue squares) maps the discrete progression of the target tube voltage, stepping from 57 kV to 69 kV. The right vertical axis (dashed orange circles) presents the system's measured accuracy percentage for each corresponding set-point. As indicated by the zoomed scale on the right axis, the system maintains high fidelity, with accuracy deviating by less than 2% across the entire operational range. The dip observed at the 60kV and 66kV set-points corresponds to the quantization error inherent in the ADC hardware, yet remains within acceptable tolerance limits. This deviation is attributed to the bit-resolution limits of the ADC hardware. Nevertheless, all output values remained well within safety tolerances. The system consistently produced the correct voltage tier for every BMI input. This confirms the robustness of the adaptive algorithm.

CONCLUSION

This study successfully engineered and validated a simulated interface for automating radiographic parameter selection. By fusing optical, gravimetric, and thermal sensors, the system effectively eliminates the subjectivity inherent in manual anthropometry. The experimental results confirm the robustness of the proposed architecture. The biometric acquisition module demonstrated clinical viability, with vertical ranging achieving absolute consistency with reference standards. Similarly, the gravimetric subsystem maintained an accuracy rate exceeding 97% across all weight classes,

despite a minor systematic offset. Crucially, the implementation of the AMG8833 thermal stability lock proved essential in preventing premature measurements, thereby reducing potential motion artifacts.

The integration of these inputs into the adaptive control logic yielded precise electronic responses. The simulation confirmed that the interface could drive a capacitor discharge circuit to distinct target voltages ranging from 57 kV to 69 kV. The telemetry data indicated that the deviation between the calculated set-point and the measured output remained negligible, consistently falling below 2%. This performance satisfies the safety tolerances required for diagnostic X-ray generators.

Currently, this research fulfills the criteria for Technology Readiness Level 3 (TRL 3), establishing a solid analytical proof-of-concept. The system validates the feasibility of using direct BMI data to drive high-voltage control circuits. Future development will focus on the transition from simulation to a physical high-voltage prototype. This next phase will involve calibrating the machine-specific correction factors against real-world X-ray output. Ultimately, this innovation promises to standardize radiation doses, minimize the necessity for image retakes, and significantly enhance patient safety in routine radiographic examinations.

REFERENCES

1. Zierle-Ghosh A, Jan A. Physiology, Body Mass Index. In: StatPearls [Internet]. Updated 2023 Nov 5. Treasure Island (FL): StatPearls Publishing; 2025. Available from: https://www.ncbi.nlm.nih.gov/books/NBK535456/
2. World Health Organization. Body mass index [Internet]. Geneva; 2023. Available from: https://www.who.int/data/gho/data/themes/topics/topic-details/GHO/body-mass-index
3. Tan KCB, others. Appropriate body-mass index for Asian populations and its implications for policy and intervention strategies. The lancet. 2004;
4. Dolenc L, Petrinjak B, Mekiš N, Škrk D. The impact of body mass index on patient radiation dose in general radiography. Journal of Radiological Protection. 2022;42(4):41505.
5. Inoue Y, Itoh H, Nagahara K, Hata H, Mitsui K. Relationships of radiation dose indices with body size indices in adult body computed tomography. Tomography. 2023;9(4):1381–92.
6. Aisah AN, Sutapa IGN, Wendri N. Penentuan Dosis Paparan Radiasi Pesawat Sinar-X Pemeriksaan Thorax Berdasarkan Indeks Massa Tubuh (IMT). Kappa Journal. 2021;5(2):240–5.
7. Metaxas VI, Messaris GA, Lekatou AN, Petsas TG, Panayiotakis GS. Patient dose in digital radiography utilising BMI classification. Radiat Prot Dosimetry. 2019;184(2):155–67.
8. Sari NLK, Prataminingsih P, Santoso B. Evaluasi Indeks Massa Tubuh (IMT) sebagai Dasar Penentuan SSDE (Size-Specific Dose Estimate) pada Pemeriksaan CT Scan Abdomen. Jurnal Fisika. 2022;12(2):76–82.
9. Wijaya NH, Sukwono D, others. Wireless X-ray Machine Control Based on Arduino with Kv Parameters. In: Journal of Physics: Conference Series. 2020. p. 12040.

10. Wijaya NH, Yudhana A, Sukwono D, others. X-Ray machine control with wireless based on mA parameters. In: IOP Conference Series: Materials Science and Engineering. 2021. p. 12080.
11. Sulistiyadi AH, Rochmayanti D, Wibowo AS. Bluetooth and Microcontroller Enabled Wireless Exposure Switch Development for X-ray Mobile Unit to Improve Radiation Protection. In: International Conference on Electronics, Biomedical Engineering, and Health Informatics. 2023. p. 481–92.
12. Loniza E, Riyadi S, Aditama HB, Chairunnisa K. Prototype of wireless Kv control system on x-rays machine. In: AIP Conference Proceedings. 2023. p. 100006.
13. Baladad BMS, Magsombol J V, Roxas JNB, De Castro EL, Dolot JA. Development of automated body mass index calculation device. Int J Appl Eng Res. 2016;11(7):5195–201.
14. Owolabi IE, Akpan VA, Oludola OP. A Low-Cost Automatic Body Mass Index Machine: The Design, Development, Calibration, Testing and Analysis. International Journal of Biomedical and Clinical Sciences. 2021;6(3):100–19.
15. Krisnadi DI, Ridwanto A. Rancang Bangun Alat pengukur Indeks Massa Tubuh (IMT) Berbasis Android. JOULE: Jurnal ilmiah Teknologi Energi, Teknologi Media Komunikasi dan Instrumentasi Kendali. 2021;1(1):16–24.
16. Faradisa IS, Muhammad RP, Girindraswari DA. A design of body mass index (BMI) and body fat percentage device using fuzzy logic. Indonesian Journal of Electronics, Electromedical Engineering, and Medical Informatics. 2022;4(2):94–106.
17. Hasan MM, Hossain ML, Junayer MJH, Alam N. An IoT-Based Calculator for Body Mass Index Determination. In: 2024 IEEE International Conference on Signal Processing, Information, Communication and Systems (SPICSCON). 2024. p. 1–4.
18. Hapsari JP, Lestari Y, Rohman SN, Al Farisi A, Angelia N. Perancangan Modifikasi Alat Antropometri sebagai Solusi Ketepatan Pengukuran Berbasis Sensor Ultrasonik. Jurnal Akademik Pengabdian Masyarakat. 2024;2(4):110–7.
19. Umiatin U, Indrasari W, Taryudi T, Dendi AF. Development of a Multisensor-Based Non-Contact Anthropometric System for Early Stunting Detection. Journal of Sensor and Actuator Networks. 2022;11(4):69.
20. Ridhani FD, Ahniar NH, Usman AI, Putra MPAT, Atmadja S. The Design of Infant Warmer with Simple Blue Light Therapy LED Addition. Sanitas. 2022;13(1):44–55.
21. Ridhani FD. Purwarupa Penghangat Bayi Dengan Elemen Pemanas Keramik, Sensor Thermopile AMG8833 dan ESP32. 2020;
22. Ridhani FD, Pritasari P, Anggraini DR. Isi Piringku Dietary Meal Proportion Estimator Applications Using SeeFood Image Segmentations. Sanitas. 2021;12(2):115–30.
23. Ridhani FD. Automated Waste Collection Container Lid Opener Prototype with Disinfectant Sprayer as Part of Nosocomial Infection Prevention. Sanitas. 2021;12(1):1–14.